JOURNAL OF APPLIED ELECTROCHEMISTRY 25 (1995) 441–449

Study of Taylor–Couette flow using a three-segment electrodiffusion probe

V. SOBOLÍK

Institute of Chemical Process Fundamentals, Academy of Sciences of the Czech Republic, 16502 Prague 6, Czech Republic

B. BENABES, G. COGNET

LEGI, Institute of Mechanics, B.P. 53 X, 38041 Grenoble Cedex, France

Received 28 June 1994; revised 19 October 1994

The axial and azimuthal components of the shear rate on the wall of the outer fixed cylinder of a pair of concentric cylinders with the inner cylinder rotating was measured using a three-segment electrodiffusion probe. The axial distribution of the components was found by sweeping vortices past the probe by means of a small axial flow. A nonzero axial shear rate component indicated the onset of Taylor vortices. Azimuthal waves on the vortices caused fluctuations of both components. The instabilities were measured in two geometries characterized by $R_1/R_2 = 0.84$ and 0.7. The probe was calibrated in the same apparatus with $R_1/R_2 = 0.94$. The Stuart theory for the growth of vortex velocity with angular velocity agrees well with the amplitude of the fundamental mode measured with $R_1/R_2 = 0.84$. Qualitative agreement was found with the numerical results of Fasel and Booz, especially between the axial shear rate component measured with $R_1/R_2 = 0.7$ and the vorticity calculated for $R_1/R_2 = 0.5$.

1. Introduction

The nature of the transition between laminar flow and fully developed turbulence is still poorly understood. Due to the complexity of this problem, it is convenient to confine investigations of transitional flows to situations with an extended region of transition. The well known Taylor–Couette flow realized between concentric rotating cylinders is the best and most studied situation. This geometry is particularly appealing because experiments can be conducted on small closed systems.

The steady laminar flow between concentric rotating cylinders becomes unstable when the rotational speed of the inner cylinder is above a critical value. The other parameters (density, radius, gap width, speed of the outer cylinder), grouped in the Taylor number, also play a role in the instability. At the first transition, a new circumferential flow with superimposed cellular, toroidal counter-rotating vortices replaces the original laminar Couette flow. Ultimately the vortices become stable and regularly spaced along the cylinder axis. At higher speed, a second transition occurs where periodic azimuthal waves are superimposed on the vortices.

Rayleigh [1] established a simple criterion for inertial instability of inviscid fluids. According to this criterion the flow is stable if, and only if, the angular momentum increases monotonically outward. Taylor [2] solved the linearized Navier–Stokes equations for small disturbances and narrow gap. The linear theory predicts the onset of Taylor vortices and their wavelength and states that the disturbances grow exponentially with time. Stuart [3] improved the analysis using non-linear instability theory for a narrow gap, $R_1/R_2 \to 1$. Davey [4] solved the governing equations using a perturbation expansion technique and tabulated velocity amplitudes for the special cases $R_1/R_2 \to 1$ and $R_1/R_2 = 0.5$. Fasel and Booz [5] used an implicit finite-difference method to investigate the Taylor-vortex flow in a wide gap, $R_1/R_2 = 0.5$, for large supercritical Taylor numbers. Their detailed analysis of velocity components, stream function, vorticity and pressure strongly supports the concept of an evolving jetlike structure when the Taylor number is increased. Spectral decomposition of the flow quantities has shown that a relatively large number of higher harmonic components are required to resolve the strong changes of the flow field for large Taylor numbers.

Taylor–Couette flow has also been investigated experimentally as indicated in the review papers by Friebe [6], Di Prima and Swinney [7] and Cognet [8]. The most frequently used methods are flow visualization and torque measurement. Unfortunately neither of these methods gives velocity distribution. Donnelly and Schwarz [9] measured the radial

0021-891X

component of the velocity field at the outer cylinder by the ion conduction technique. These measurements were only relative, that is, it was difficult to obtain absolute values. Snyder and Lambert [10] used a thermistor anemometer embedded in the inner cylinder for the measurement of the shear rate. This method is incomplete in the following aspects. At small Peclet number the sensitivity of the anemometer to the velocity field is low. Only about 10% of the total energy input is transmitted by the anemometer to the fluid and hence used for the shear measurement. The other part of the energy is transmitted into the cylinder and is then lost in the fluid. The excess temperature of about 6 °C may cause thermal instability of the flow. For measurement of the axial dependence of the shear rate, Snyder and Lambert [10] swept the Taylor cells past the thermistor using a small axial flow. Gollub and Freilich [11] measured the radial velocity component by the laser Doppler technique. Eisenberg *et al.* [12] and Mizushina *et al.* [13] used the electrodiffusion technique for measurements of the local mass transfer rate on the surface of the outer cylinder. Cognet [14] and Bouabdallah and Cognet [15] used the same technique, but interpreted the results as shear rate. Using a simple probe they estimated the magnitude of the shear rate and studied the axial dependence of the spectral density of the fluctuations. Fenstermacher *et al.* [16] used the laser Doppler technique for spectral analysis of the radial velocity component in the azimuthal wavy flow regime.

Due to limitations in the above mentioned measuring technique, only the absolute value of the shear rate or a single velocity component was measured. The only exception is the work of Muller *et al.* [17], who used two component laser Doppler velocimetry for the measurement of the onset of instability in viscoelastic Couette flow. However, they presented only purely elastic oscillations of the axial velocity component in a Boger fluid and no data in Taylor–Couette flow.

It is convenient to study disturbances by the measurement of the local shear rate on the cylinder wall. In opaque liquids it is the only applicable method. To obtain more information about the flow field it is necessary to decompose the absolute value of the shear rate into axial and azimuthal components.

The electrodiffusion method, based upon the measurement of the limiting diffusion current on a working electrode, is a very efficient method for the evaluation of shear stress or shear rate [12–15, 18]. Rectangular and circular probes [19, 20], composed of two parts separated by a thin insulation gap, were used for the measurement of the flow direction. The maximum angle resolution is 180° with bicircular probes [20]. The angle resolution with a square probe composed of four small square electrodes [21] is quite good, but the total current depends on the flow direction. Recently developed three-segment circular probes [22–26] have a very good angular resolution in the whole interval 0–360° and the total current is independent of the flow angle. With this probe embedded in the wall of the outer cylinder it is possible to measure the azimuthal and axial components of the shear rate in Taylor–Couette flow simultaneously, without any interference with the flow.

The advantages of the use of this probe in disturbed Couette flow will be shown in the present paper. The onset of Taylor vortices and azimuthal waves will be determined by computerized experiments. The axial distribution of the axial and azimuthal components of the shear rate will be measured by sweeping the fully developed vortices past the probe at different rotation speeds.

2. Theory

2.1. *Three-segment electrodiffusion probes*

The measurement of the wall shear stress or shear rate by means of the limiting diffusion current is a well-known technique [13, 18, 19], based on the following principle. A two-electrode cell consisting of a small working electrode and a larger auxiliary electrode is used and the solution contains electroactive species and excess supporting electrolyte. The velocity field very close to the working electrode controls the species transport and, thus, the measured current. In this region the velocity field can be approximated by a linear dependence on the normal distance from the surface, y, with the shear rate, γ, a coefficient of proportionality. If the Peclet number ($Pe = \gamma L^2/D$) is sufficiently high, then the current density obeys the relation

$$i = Kx^{-1/3} \tag{1}$$

where x is measured from the electrode leading edge, K depends on the number of electrons n involved in the reaction of one ion.

Now,

$$K = \frac{nFc_0D^{2/3}(\gamma/9)^{1/3}}{\Gamma(4/3)} \tag{2}$$

where F is the Faraday constant, c_0 is the bulk active species concentration, D is the diffusion coefficient, and γ is the shear rate. Integration of Equation 1 yields the total current for a circular electrode of radius R,

$$I = 4.007\,K\,R^{5/3} \tag{3}$$

and for a rectangular electrode with length L and width W,

$$I = 1.5\,KWL^{2/3} \tag{4}$$

Hence the total current depends on the electrode length to the power 2/3. Segmented electrodes make use of this fact for the resolution of the flow direction. A circular electrode composed of three isolated segments is shown in Fig. 1. The principle of the flow angle resolution is as follows. The current I_1

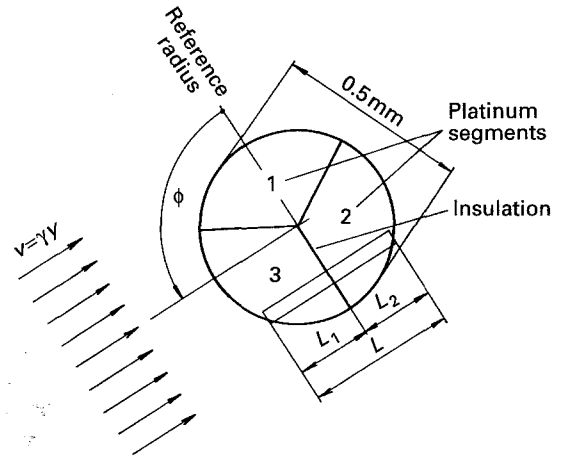

Fig. 1. Three-segment electrodiffusion probe.

through the upstream part L_1 of the strip L is greater than the current I_2 through the downstream part L_2. Making use of Equation 4 for the current ratio

$$I_1/I_2 = I_1/(I - I_1) = L_1^{2/3}/(L^{2/3} - L_1^{2/3}) \quad (5)$$

For example, for $L_1 = L_2$ it follows that $I_1 = 1.59\,I_2$. Hence the current at a segment of a circular electrode depends on the flow angle ϕ and γ, whereas the sum of the currents depends only on γ. For calculation of the flow direction it is convenient to normalize the segment currents by their sum. Then the normalized currents depend only on ϕ. We term the dependencies $I_j/\Sigma I_k = f_j(\phi)$ the directional characteristics. More information about three-segment probes can be found in [23–27]. As the three-segment probes manufactured up to the present are not geometrically perfect, it is necessary to calibrate them. The most frequently used method is to adjust the flow angle by turning the probe in a viscometric flow field and measure the segment currents. The measured dependence of the normalized segment currents on the flow angle are then approximated by Fourier series. As the electrode surface area and the diffusion coefficient are not exactly known, the dependence I–γ should be measured in the same solution as that used in the experiment. Another reason for this recommendation is the parallel reaction of dissolved oxygen which increases the measured current above the value corresponding to the concentration of the intended electroactive species.

2.2. *Velocity distribution in Taylor–Couette flow*

For two concentric rotating cylinders, with r, θ, z as the cylindrical coordinates and v_r, v_θ, v_z the corresponding velocity components, the flow has axial symmetry and is, therefore, independent of θ. When the rotational speed of the inner cylinder is above a critical value, laminar flow is no longer stable and disturbances appear which ultimately take the form of cellular, toroidal vortices, regularly spaced along the axis, z, of the cylinders. A Taylor vortex and the coordinate system are shown in Fig. 2. The velocity components of a stable vortex are periodic functions of z:

$$v_r(r,z) = \sum_k v_{rk}(r)\cos k[\alpha z + \varphi_{rk}(r)] \quad (6)$$

$$v_\theta(r,z) = \overline{v_\theta}(r) + \sum_k v_{\theta k}(r)\cos k[\alpha z + \varphi_{\theta k}(r)] \quad (7)$$

$$v_z(r,z) = \sum_k v_{zk}(r)\sin k[\alpha z + \varphi_{zk}(r)] \quad (8)$$

According to the numerical solution [5] the phases $\varphi_{ik}(r)$ have either of the values $0, \pi/k$,

Under the assumption that the mean velocity $\overline{v_\theta}(r)$ is the same as in laminar Couette flow, linear theory [28] predicts the critical Taylor number and wave number α. Nonlinear theory [3, 4] takes into account the distortion of the mean flow by disturbances. Under the assumption that α is known from linear theory, Stuart [3] found the dependence of the fundamental mode, i.e. $v_{r1}(r)$, $v_{\theta 1}(r)$ and $v_{z1}(r)$ on the Taylor number. Davey [4] calculated the amplitudes v_{rk} and $v_{\theta k}$ for $k = 1, 2, 3$ by a perturbation expansion technique. Fasel and Booz [5] obtained a complete velocity field $v_r(r,z)$, $v_\theta(r,z)$ and $v_z(r,z)$ including the pressure and vorticity distribution by an implicit finite difference method.

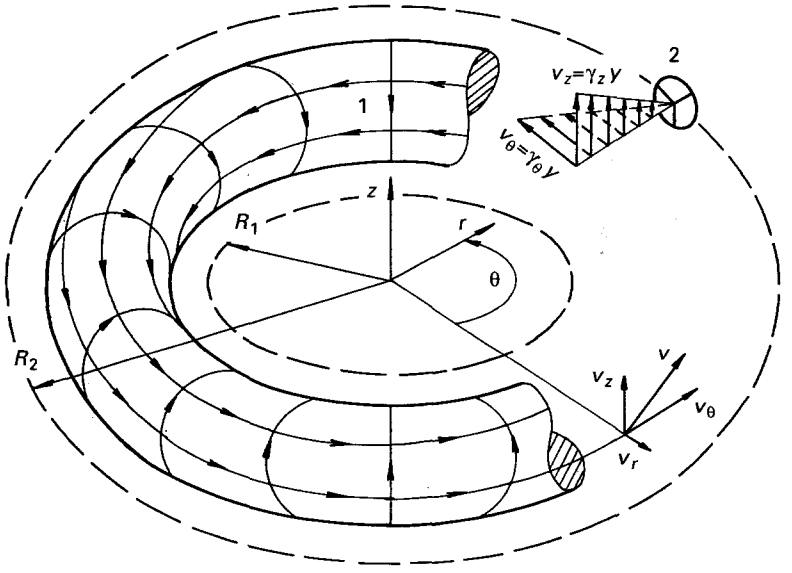

Fig. 2. Structure of a Taylor vortex. (1) stream tube and (2) three-segment electrodiffusion probe.

Under the assumption that the velocity field close to the electrode can be linearized and that the streamlines are almost parallel lines, the shear rate measured by a three-segment electrodiffusion probe can be decomposed into two components [23–26]. At the wall of the outer fixed cylinder, these components can be calculated from the velocity components, Equations 7 and 8.

$$\gamma_\theta(z) \equiv \left.\frac{\partial v_\theta}{\partial r}\right|_{r=R_2} = \overline{\gamma_\theta} + \sum_k \gamma_{\theta k} \cos k[\alpha z + \varphi_{\theta k}(R_2)] \tag{9}$$

$$\gamma_z(z) \equiv \left.\frac{\partial v_z}{\partial r}\right|_{r=R_2} = \sum_k \gamma_{zk} \sin k[\alpha z + \varphi_{zk}(R_2)] \tag{10}$$

where

$$\overline{\gamma_\theta} = \left.\frac{\partial \overline{v_\theta}}{\partial r}\right|_{r=R_2} \tag{11a}$$

$$\gamma_{\theta k} = \left.\frac{\partial v_{\theta k}}{\partial r}\right|_{r=R_2} \tag{11b}$$

$$\gamma_{zk} = \left.\frac{\partial v_{zk}}{\partial r}\right|_{r=R_2} \tag{11c}$$

The phases $\varphi_{ik}(R_2)$ were found to be zero [5].

Fasel and Booz [5] calculated the vorticity at the walls of the inner and outer cylinders from

$$\Omega(r,z) = -\left.\frac{\partial v_z}{\partial r}\right|_{r=R_1,R_2} \tag{12}$$

Hence the axial shear rate component, $\gamma_z(z)$, is equal to the vorticity, $\Omega(R_2, z)$.

It follows from Equations 9–11 that the theoretical predictions for the velocity field can be checked by measurement of γ_θ and γ_z. On the other hand the measured distribution of γ_θ and γ_z can be used as boundary conditions for calculation of the velocity distribution.

3. Experimental details

The fluid was contained between two plexiglass cylinders. The outer fixed cylinder had a radius, R_2, of 30.6 mm, and the inner interchangeable cylinders had radii, R_1, of 28.8, 25.6 and 21.4 mm. The corresponding ratio $\eta = R_1/R_2$ was 0.94, 0.84 and 0.7. The gap between cylinders had a length of 140 mm. Assuming that a vortex has a height equal to the width of the gap, 28 and 15 vortices could be accommodated in the apparatus with $\eta = 0.84$ and 0.7, respectively. The inner cylinder was coupled by a flexible tube with the shaft of a gear box which was mounted on an electromotor with adjustable rate of rotation. Two endless screws in the gear box produced a rotation reduction ratio of 1:121. The rotation rate was measured by means of a tachometer coupled to the electromotor shaft. The rotation rate of the inner cylinder could be adjusted in the range 0.6–36 rpm.

The three-segment electrodiffusion probe was made in house. Three platinum wires with a diameter of 0.5 mm were pulled simultaneously through a wire-drawing die, starting with a die diameter of 1 mm and finishing with 0.5 mm. This caused the originally circular wires to take a cross-section shape as shown in the segments 1, 2 and 3 in Fig. 1. The wires were then coated electrophoretically with a deposit of a polymeric paint and glued together with Araldite. After soldering the connecting cables, the probe was glued with Epoxide Resin (product of Buehler) into a stainless steel tube with a tip diameter of 3 mm. The face of the tube was then polished with emery paper of a grit size 15 μm. The stainless steel tube served as anode. The three-segment electrodiffusion probe was flush mounted into the wall of the outer cylinder at a distance of 65 mm below the top of the inner cylinder.

The test fluid was a 10 mol m^{-3} equimolar potassium ferri/ferrocyanide aqueous solution with 100 mol m^{-3} K_2SO_4 as supporting electrolyte. The density of the solution was 1020 kg m^{-3} and the kinematic viscosity was 1.02×10^{-6} m^2 s^{-1} at 22 °C.

Vortices were swept over the probe using a low axial flow generated by a driven syringe. The mean velocity was 0.07 mm s^{-1} in the 5 mm gap and 0.09 mm s^{-1} in the 9.2 mm gap. The corresponding Reynolds number and the shear rate of the superposed axial motion were smaller than 1.8 and 0.1 s^{-1}, respectively.

The probe was calibrated in laminar Couette flow generated by the largest cylinder. The electrochemical system was initially checked by measuring polarization curves at different shear rates, see Fig. 3. The curves exhibited good plateaux. During calibration the shear rate was adusted in the range 0.85 to 36 s^{-1}. A potential drop of −0.6 V was then imposed between the electrodes. As the Peclet number is too small, due to low shear rates, the experimentally found dependence I–γ does not obey the power law with the theoretical power 1/3, see Fig. 4. Hence the empirical relation

$$I = 1.831\,\gamma^{1/3} + 0.460\,\gamma^{-1/3} - 0.152\,\gamma^{-1/6} \tag{13}$$

was used for the evaluation of $\gamma(s^{-1})$ from the

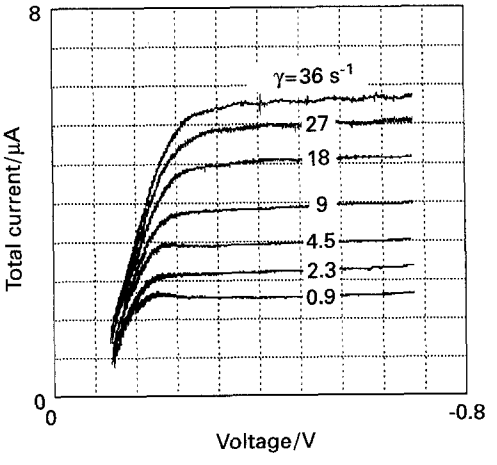

Fig. 3. Polarization curves at different shear rate.

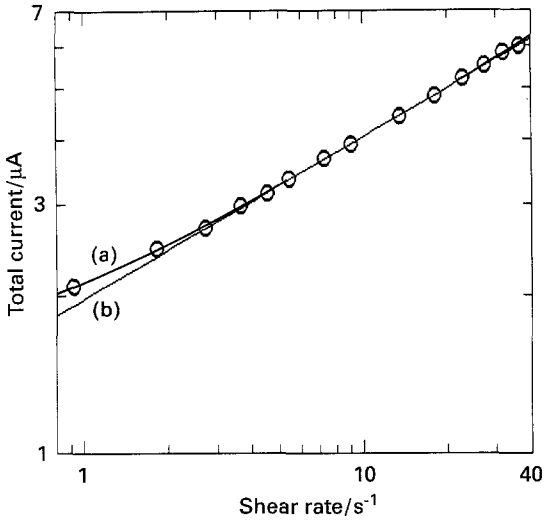

Fig. 4. Dependence of total current on shear rate. (a) Equation 13, and (b) power law dependence $I = K\dot{\gamma}^n$ with $n = 0.31$ and $K = 1.99$.

measured total current $I(\mu A)$. A similar relation was proposed by Dimopoulos and Hanratty [29], however here the multiplying coefficients were obtained by a least squares fit of the experimental data.

The directional characteristics of the probe were obtained in the following way. By turning the probe around its axis in laminar Couette flow, the flow angle was adjusted in steps of 15°. For each angle the three segment currents were measured and the total current, I, and normalized currents, I_j, were calculated by dividing the currents by the total current. The dependencies of the normalized currents on the flow angle ϕ were fitted by Fourier series, see Fig. 5. The directional characteristics were practically independent of the shear rate. For the measurements the reference radius of the probe was chosen at 270°. In other words the flow angle 270° pointed in the azimuthal direction.

The calibrations and measurements were fully computerized. A 80486 computer was connected by means of an A/D and D/A board with an electrodiffusion analyser. The home made analyser supplied the

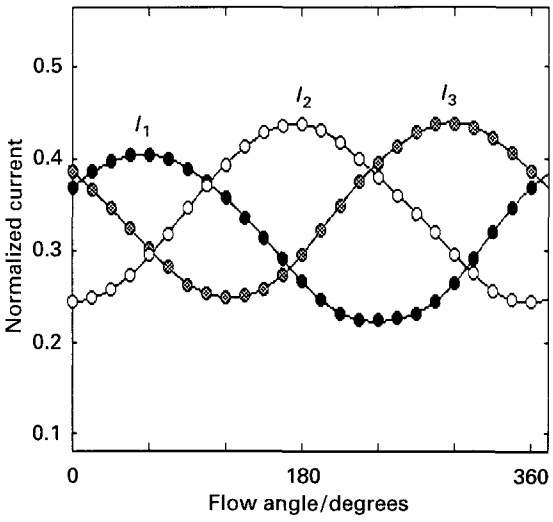

Fig. 5. Directional characteristics of three-segment electrodiffusion probe.

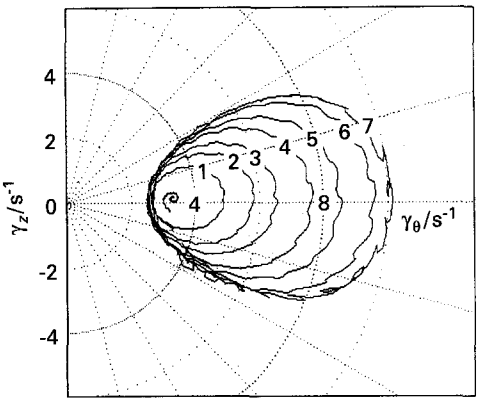

Fig. 6. Phase diagram γ_z–γ_θ in the narrow gap, $\eta = 0.84$. ω/ω_c: (1) −1; (2) −1.04; (3) −1.07; (4)−1.11; (5) −1.18; (6) −1.26; and (7) −1.30.

same voltage on all the segments and measured the limiting currents. The sampling frequency of the segment currents was 2000 Hz. The instantaneous values of γ_θ and γ_z were calculated on-line and their mean values and standard deviations, together with current time, were recorded every 0.9 s. A phase plot on the screen with γ_θ on the abscissa and γ_z on the ordinate was used for investigating disturbances in the Couette flow, see Figs 6 and 7. A point with coordinates γ_θ and γ_z is the end point of a vector parallel with the flow direction having magnitude equal to the shear rate. In laminar flow γ_z is zero and the corresponding points lie on the abscissa. With the exception of the source and sink, the secondary motion manifests itself by a nonzero γ_z. If the flow is steady, the point does not move. Any closed line corresponds to a pair of steady, fully developed vortices. When more than two vortices were swept over the probe by the mean axial flow, identical curves were obtained. Hence the neighbouring vortices have the same velocity distribution. The small spiral curve in the middle of Fig. 6 shows the onset of Taylor vortex. It expresses the time evolution of the growing vortex towards state 1 ($\omega/\omega_c = 1$, Fig. 6).

4. Results and discussion

As the time histories of $\gamma_z(t)$ and $\gamma_\theta(t)$ were recorded during one experiment it was possible to calculate

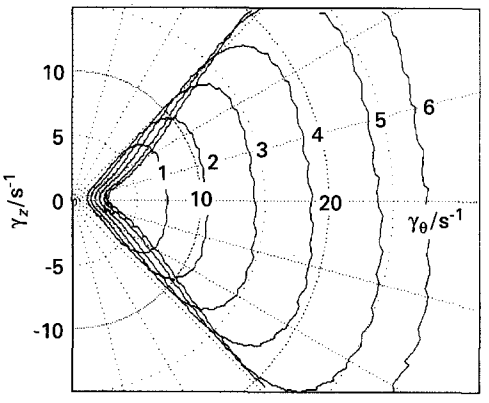

Fig. 7. Phase diagram γ_z–γ_θ in the wide gap, $\eta = 0.7$. ω/ω_c: (1) −3.33; (2) −4.17; (3) −5.00; (4) −5.83; (5) −6.67; and (6) −7.50.

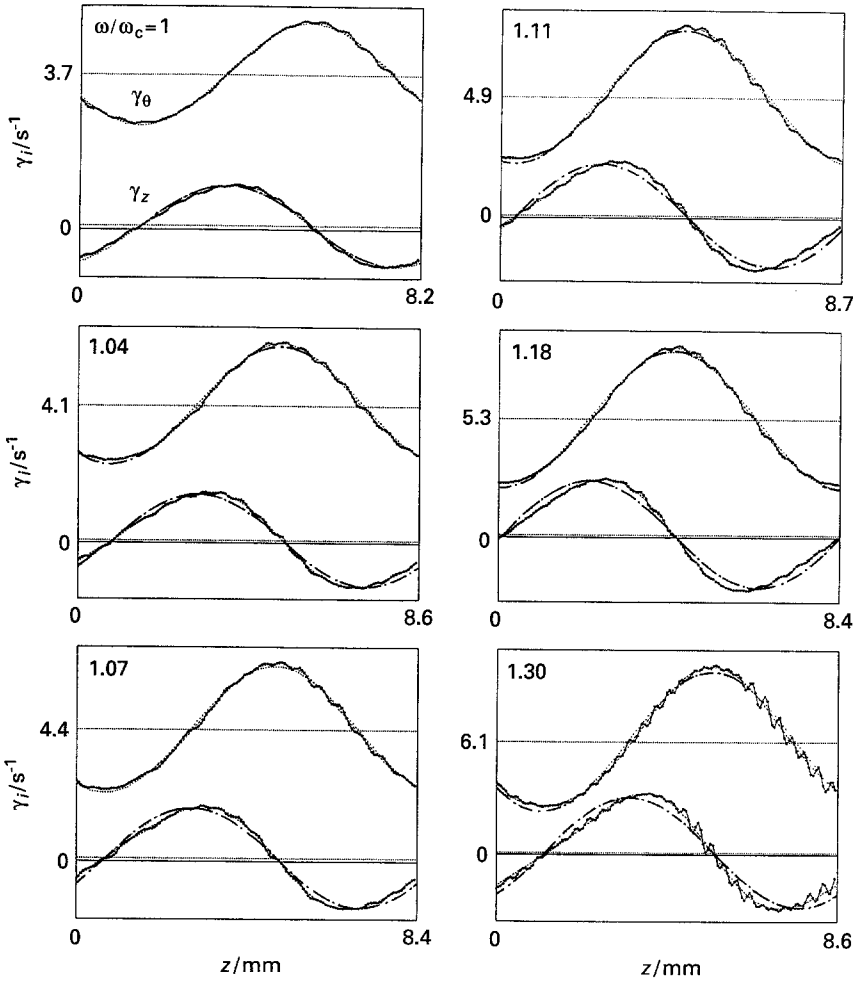

Fig. 8. Dependence of γ_z and γ_θ on z for $\eta = 0.84$.

$\gamma_z(z)$ and $\gamma_\theta(z)$ by means of the known sweeping velocity. Typical dependencies are shown in Figs 8 and 9 for η equal to 0.84 and 0.7. The origin is arbitrary and depends on the relative position of the vortex and probe at the start of measurement. The scales of the ordinates and abscissas depend on the shear rate and wavelength of each vortex. The mean values of the shear rate components are marked by thin horizontal straight lines. The value of $\overline{\gamma_\theta}$ and the wavelength are given at the appropriate axis. The value of $\overline{\gamma_z}$ should be equal to the sweeping shear rate, i.e., $0.09\,s^{-1}$ for $\eta = 0.84$ and $0.06\,s^{-1}$ for $\eta = 0.7$. The number in the upper left corner of each diagram represents the angular velocity normalized by the angular velocity of the onset of Taylor vortices, ω/ω_c. The critical velocity ω_c was equal to $0.785\,rad\,s^{-1}$ for $\eta = 0.84$ and $0.35\,rad\,s^{-1}$ for $\eta = 0.7$. The dashed and dotted curves present the first harmonics. The second harmonics are denoted by the thin curves. At $\omega/\omega_c = 1.3$ azimuthal waves appeared on Taylor vortices in the small gap. They manifested themselves by periodical dependencies of γ_θ and γ_z on time. Because the averaging time of one measurement (0.9 s) is smaller than the wave period (approximately 4.6 s), periodic fluctuations appeared in the phase diagram and dependencies $\gamma_\theta(z)$ and $\gamma_z(z)$, see Fig. 6 and the last diagram in Fig. 8. For a narrower gap, $\eta = 0.908$, Cognet [14] obtained a value of 1.2. No azimuthal waves occur even at $\omega/\omega_c = 9.2$. For $\eta = 0.5$ Snyder and Lambert [10] found the Taylor vortices steady even at $\omega/\omega_c = 10$.

From the theory of Taylor vortices it follows that the axial velocity is zero and changes direction in the planes separating neighbouring vortices. The radial velocity in these planes is directed either towards or away from the outer wall. Hence the radial velocity creates either a source or sink at the outer wall. The azimuthal velocities near the outer wall have maxima in the planes of the source and minima in the planes of the sink. These facts were confirmed by numerical study [5], see Fig. 7 (c) (d) and (e). Hence the radial gradient of the azimuthal velocity has a maximum in the source and minimum in the sink. The radial gradients of the axial velocity are zero in both source and sink.

As the numerical study [5] was done for $\eta = 0.5$, only qualitative comparison with our results is possible. From the distribution of azimuthal velocity shown in Fig. 7(d) of [5] it follows that the radial gradient of the azimuthal velocity, γ_θ, has a maximum in the source and a minimum in the sink. This is in agreement with the results shown in Figs 8 and 9, where the maxima and minima of γ_θ correspond to $\gamma_z = 0$. There is also qualitative agreement between the forms of $\gamma_z(z)$ in Fig. 9 and the vorticity $\Omega(R_2, z)$ shown in Fig. 8(j) of [5]. Figure 9 documents great changes of the flow field with increasing *Re* and a jet like, or in other words, boundary layer character of the flow at high rotation rates. Whereas $\gamma_z(z)$ and

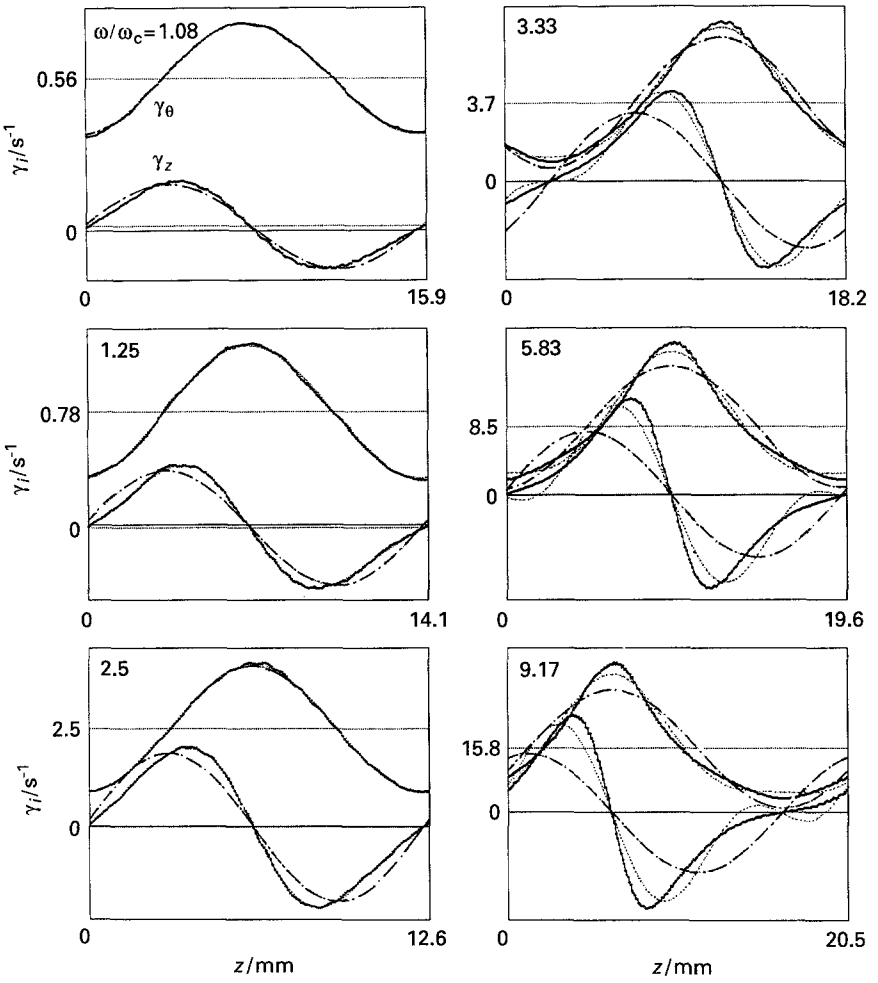

Fig. 9. Dependence of γ_z and γ_θ on z for $\eta = 0.7$.

$\gamma_\theta(z)$ have nearly sinusoidal form just beyond the critical rotation rate, they exhibit more pronounced peaks with increasing rotation rate. The $\gamma_z(z)$ peaks are not in the central plane of the vortex, but they are closer to the source, the higher the rotation rate.

The amplitudes γ_{zk} and $\gamma_{\theta k}$ of harmonics, defined in Equations 9–11, were found by Fourier decomposition of the measured data. Amplitudes of the fundamental mode, first harmonic ($k = 1$), and higher harmonics up to the order 4 are shown in Fig. 10 for $\eta = 0.84$. Series with terms of order $k = 2$ are sufficient for good fit, because the amplitudes of the third harmonic are about 1% of the first ones. The higher harmonics are not significant until the appearance of azimuthal waves. There is very good agreement with the Stuart theory [3]. The significance of the harmonics in the wide gap, $\eta = 0.7$, is obvious from Fig. 11. Two regions can be distinguished with different slope. The break point is at about $\omega/\omega_c - 1 = 1$, and corresponds approximately to the

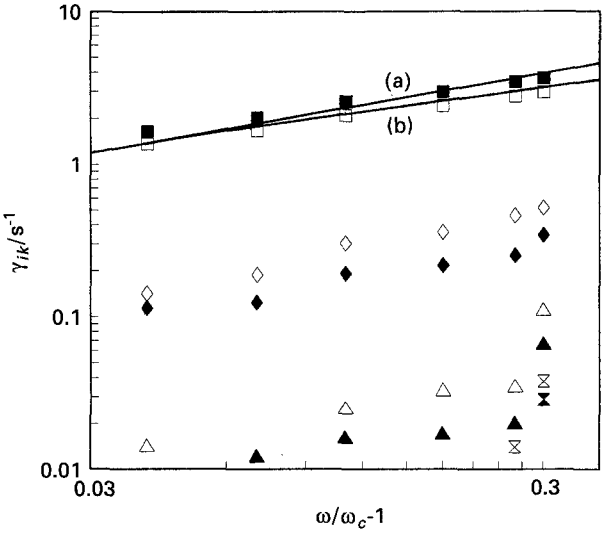

Fig. 10. Amplitude growth of fundamental mode and harmonics for $\eta = 0.84$.. Stuart [3] solution for (a) $\gamma_{\theta 1}$ and (b) γ_{z1}. Key: (■) $\gamma_{\theta 1}$, (◆)$\gamma_{\theta 2}$, (▲) $\gamma_{\theta 3}$, (⧗) $\gamma_{\theta 4}$, (□) γ_{z1}, (◇) γ_{z2}, (△) γ_{z3}, (⧖) γ_{z4}.

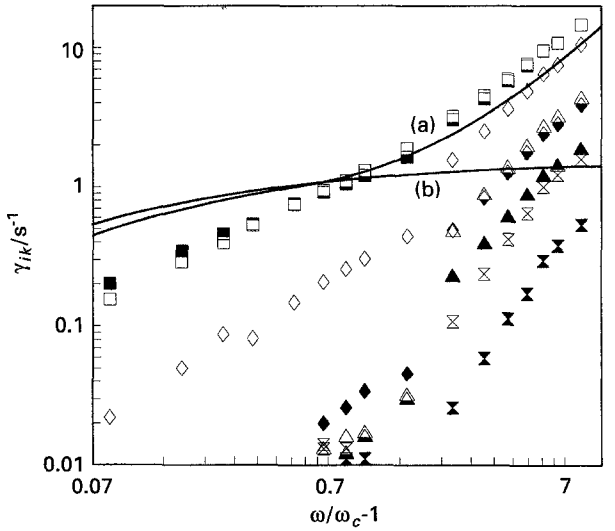

Fig. 11. Amplitude growth of fundamental mode and harmonics for $\eta = 0.7$. For legend see Fig. 10.

vortex with the smallest wave length, $\lambda = 12.6$ mm, shown in Fig. 9. At smaller angular velocity, only the second harmonics, γ_{z2}, having a value of 10% of the fundamental mode, is not negligible. At higher rotation rate higher harmonics become significant. Gollub and Freilich [11] also found a break point, but only the slope of the fundamental mode amplitude was greater at greater angular velocity. For $\eta = 0.7$ the theory [3] does not fit the experimental data at all because it was derived for a narrow gap.

For comparison of γ_{zk} with the harmonics of vorticity shown in Fig. 11(d) of [5], the harmonics γ_{zk} are plotted in semilogarithmic coordinates in Fig. 12. There is good qualitative agreement with the only exception being the third harmonic at small rotation rate. Its local minimum may be explained by the finite sensitivity of the probe.

If the normal velocity component exists at the wall, the wall shear rate is not more homogeneous. The directional characteristics measured in the presence of the normal velocity component differs from that in a steady homogeneous flow [25, 30]. A parameter κ was introduced which stands for the ratio of the maximum difference of the wall shear rate at the centre and boundary of a probe. The value of κ varies between 1, this value corresponds to a flow with stagnation point on the probe boundary, and 0, corresponding to a homogeneous flow without normal velocity component. Because γ_θ has finite values in the planes going through sources and sinks where the radial component is significant, κ does not reach large values. The maximum of 0.12 was estimated for $\max(\gamma_\theta)$ and $\gamma_z = 0$, i.e in the source on the last diagram in Fig. 9. Because even this, in our experiments, exceptional value has only little influence on the directional characteristics, we used the directional characteristics measured in viscometric flow for evaluation of the flow direction.

The above results show the convenience and reliability of the three-segment electrodiffusion probe for mapping of the shear rate components in Taylor–Couette flow.

It is also intended to make more systematic measurements in non-Newtonian viscoelastic liquids [31] and fibre suspensions [32] and in time dependent wavy vortex flow.

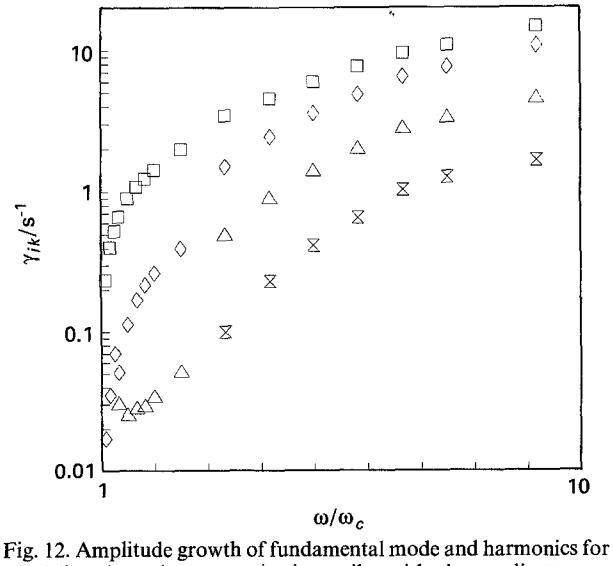

Fig. 12. Amplitude growth of fundamental mode and harmonics for $\eta = 0.7$ as dependence on ω/ω_c in semilogarithmic coordinates.

5. Conclusions

Three-segment electrodiffusion probes are very efficient tools for measurement of the azimuthal and axial wall shear rate components in Couette flow with instabilities. Directional resolution is still accurate at very low shear rates of the order $1\,s^{-1}$. The onset of Taylor vortices and azimuthal waves was identified by the computerized measuring system. Superposition of a small axial motion on the Taylor vortices makes it possible to infer the wavelength of the cells and the dependence of the shear rate components on the axial coordinate.

The amplitudes of the axial and azimuthal shear rate measured with $\eta = 0.84$ agree well with the Stuart theory for the growth of vortices in a narrow gap.

There is qualitative agreement between the axial shear rate measured with $\eta = 0.7$ and the vorticity calculated by Fasel and Booz [6] for $\eta = 0.5$, and between the measured azimuthal shear rate and calculated azimuthal velocity.

Acknowledgements

The authors express their thanks to the Rhone-Alpes region which made this work possible by scholarship TEMPRA, the Algerian French Government Scholarship Program and the Grant Agency of the Czech Republic. The contribution of Prof. O. Wein (AS CR, Prague) to the development of the software and discussion with Dr B. Lismonde (LEGI/IMG, Grenoble) is greatly appreciated.

References

[1] Lord Rayleigh, *Proc. Royal Soc., Lond. A* **93** (1916) 148.
[2] G. I. Taylor, *Phil. Trans. Roy. Soc., Lond. A* **223** (1923) 289.
[3] J. T. Stuart, *J. Fluid Mech.* **4** (1958) 1.
[4] A. Davey, *ibid.* **14** (1962) 336.
[5] H. Fasel and O. Booz, *ibid.* **138** (1984) 21.
[6] H. W. Friebe, *Rheol. Acta* **15** (1976) 329.
[7] R. C. Di Prima and H. L. Swinney, Topics in Applied Physics **45**, (edited by H. L. Swinney and J. P. Gollub), Springer Verlag, Berlin (1981) pp. 139–80.
[8] G. Cognet, *J. Mécanique Théorique et Appliquée*, Num.spéc. (1984) 7.
[9] R. J. Donnelly and K. W. Schwarz, *Proc. Roy. Soc., Lond. A* **283** (1965) 531.
[10] H. A. Snyder and B. Lambert, *J. Fluid Mech.* **26** (1966) 545.
[11] J. P. Gollub and M. H. Freilich, *Phys. Fluids* **19** (1976) 618.
[12] M. Eisenberg, C. W. Tobias and C. R. Wilke, *Chem. Eng. Prog., Symp. Ser.* **51** (1955) 1.
[13] T. Mizushina, R. Ito, S. Hiraoka, A. Ibusuki and I. Sakaguchi, *J. Chem. Eng. Japan.* **2** (1969) 89.
[14] G. Cognet, *J. Mécanique* **10** (1971) 65.
[15] A. Bouabdallah and G. Cognet, 'Laminar-Turbulent Transition', IUTAM Symposium, Stuttgart (edited by R. Eppler and H. Fasel) Springer Verlag (1984) p. 368.

[16] P. R. Fenstermacher, H. L. Swinney and J. P. Gollub, *J. Fluid Mech.* **94** (1979) 103.
[17] S. J. Muller, E. S. G. Shaqfeh and R. G. Larson, *J. Non Newt. Fluid Mech.* **46** (1993) 315.
[18] J. R. Selman and C. W. Tobias, *Adv. Chem. Engng* **10** (1978) 21.
[19] T. J. Hanratty and J. A. Campbell, 'Fluid Mechanics Measurements', (edited by R. J. Goldstein) Hemisphere, Washington DC (1983) p. 559.
[20] B. Py, *Int. J. Heat Mass Transf.* **16** (1973) 129.
[21] K. Wichterle and L. Zák, *Czech Patent AO 231 308* (1981).
[22] V. Sobolík, P. Mitschka and T. Menzel, *Czech Patent AO 262 823* (1989).
[23] O. Wein and V. Sobolík, *Collect. Czech. Chem. Commun.* **52** (1987) 2169.
[24] T. Menzel, V. Sobolík, O. Wein and U. Onken, *Chem.-Ing.-Tech.* **59** (1987) 492.
[25] O. Wein and V. Sobolík, *Collect. Czech. Chem. Commun.* **54** (1989) 3043.
[26] C. Deslouis, O. Gil and V. Sobolík, *Int. J. Heat Mass Transf.* **33** (1990) 1363.
[27] V. Sobolík, O. Wein, O. Gil and B. Tribollet, *Exp. Fluids* **9** (1990) 43.
[28] S. Chandrasekhar, 'Hydrodynamic and Hydromagnetic Stability', Dover Publications, New York (1961).
[29] H. G. Dimopoulos and T. J. Hanratty, *J. Fluid Mech.* **33** (1968) 303.
[30] F. Baleras, C. Deslouis, B. Tribollet and V. Sobolík, *J. Appl. Electrochem.* **24** (1994) 676.
[31] V. Sobolík, B. Benabes and G. Cognet, 'Progress and Trends in Rheology IV,' Proceedings of the 4th European Rheology Conference (edited by C. Gallegas), Sevilla (1994) p. 551.
[32] V. Sobolík, B. Benabes and G. Cognet, IUTAM Symposium on Liquid Particle Interactions in Suspension Flows, Grenoble (1994).